Dental Materials Journal 2022; 41(4): 608–615

Visualization of orthodontic forces generated by aligner-type appliances

Yuri SHIMADA[1], Yoshifumi YOSHIDA[2], Ryosuke ISOGAI[2] and Koutaro MAKI[1]

[1] *Department of Orthodontics, Graduate School of Dentistry, Showa University, 2-1-1 Kitasenzoku, Ota-ku, Tokyo 145-8515, Japan*
[2] *Seiko Holdings Corporation, 1-26-1 Ginza, Chuo-ku, Tokyo 104-8110, Japan*
Corresponding author, Yuri SHIMADA; E-mail: y.shimada@dent.showa-u.ac.jp

Recently, the number of patients who request esthetically pleasing aligner-type orthodontic appliances (referred to as aligners) has been increasing. However, the orthodontic forces generated by these aligners are still unknown. This study aimed to verify whether the orthodontic force in aligners can be estimated by measuring near infrared 2D birefringence, and to visualize the orthodontic force. We measured the mechanical and photoelastic properties of transparent orthodontic thermoplastic specimens to correlate the optical retardation with the applied load. The results confirmed equivalence between the mechanical properties and the photoelasticity. In addition, the 2D retardation distribution that occurred when stress was applied to the sample was mapped and visualized. This indicates that it is possible to estimate and visualize the orthodontic force using the retardation obtained by near infrared 2D birefringence measurement.

Keywords: Aligner, Thermoplastics, Orthodontic force, Near infrared 2D birefringence measurement system, Photoelasticity

INTRODUCTION

Until recently, orthodontic treatment has generally required the patient to wear a fixed appliance for a long period of time to improve malocclusion. However, some patients have tended to avoid these devices because of their poor esthetics. In recent years, as demand for orthodontic treatment among adult patients has increased[1,2], the number of patients requesting orthodontic appliances with better esthetics has increased, and various types of appliances have been developed as a result. Among these devices, aligner-type orthodontic appliances (referred to as aligners), which are made from transparent thermoplastic materials, have rapidly become popular in recent years because of their comparatively high esthetic quality[3]. In orthodontic treatment using aligners, tooth movement comprises several stages from the start of treatment to completion; the patient wears an aligner molded into the desired position after movement during each stage, and the orthodontic force is thus applied to the teeth sequentially[4,5]. Because these aligners are removable by the patient, they are reported to have advantages over fixed appliances, such as improved comfort during treatment[6], better oral hygiene, and reduced periodontal disease[7] and root resorption[8,9].

Conversely, orthodontic treatment using aligners has been reported to be inefficient in specific tooth movement and lacking in predictive feasibility[10-13]. Quantitative evaluation of the magnitude and distribution of the orthodontic force produced by aligners in individual patients is essential to clarify the causes of these problems. However, few studies have measured the orthodontic force characteristics of aligners. In previous reports, the orthodontic forces produced by aligners were measured using small force sensors, thin-film pressure sensors, and 3D force-and-moment sensors, and the effects of the thickness and the materials of the aligners on the orthodontic forces produced were verified[14-17]. However, previous methods of measuring the orthodontic forces have required modification of the models and of the aligners themselves, which raises questions about the reproducibility and accuracy of these measurements, and the results also cannot be captured visually. In addition, in previous reports, only the teeth to which the orthodontic force was to be applied were measured, meaning that the portions without sensors were not measured, and thus the effect of the orthodontic force on the entire dentition could not be evaluated. Even for the teeth with sensors, the measured pressure is actually an average value per unit sensor area, which makes it impossible to measure the high-resolution orthodontic force distribution.

Therefore, we used the photoelasticity of the aligner material to accurately measure the orthodontic force of aligners. To measure the photoelasticity of the material, we used a near infrared 2D birefringence measurement system. This equipment operates on the principle that when stress is applied to a transparent specimen onto which light has been projected, an optical retardation (hereafter referred to as retardation) is generated because of the birefringence derived from transparent polyethylene terephthalate (PET), which is a primary material of aligners, and this retardation is expected to be proportional to the applied stress[18]. This system can measure and visually evaluate the strength and distribution of the orthodontic forces acting on the entire dentition or on a single tooth surface without any undesirable processing of the aligner or the model.

The purposes of this study were: (1) to verify

Color figures can be viewed in the online issue, which is available at J-STAGE.

Received Dec 21, 2021: Accepted Feb 18, 2022
doi:10.4012/dmj.2021-330 JOI JST.JSTAGE/dmj/2021-330

whether the orthodontic force characteristics of the aligner material can be derived from photoelasticity using a near infrared 2D birefringence measurement system, and (2) to establish the basis for visualization of orthodontic forces.

MATERIALS AND METHODS

Principles of near infrared 2D birefringence measurement

Photoelasticity is a phenomenon by which a transparent elastic material temporarily exhibits both optical anisotropy and birefringence when an external force is applied to induce stress in that material[18-20]. Birefringence refers to a state in which the stressed material has two different indices of refraction (n_1, n_2) depending on the light's polarization (the direction of light vibration). In transparent materials such as glass and plastic, the value of the refractive index changes according to the amount of stress applied. This is called the stress optic law:

$$(n_1-n_2)=C(\sigma_1-\sigma_2) \quad (1)$$

where (n_1-n_2) is the difference between the indices of refraction, C is the stress-optic coefficient of the specimen, and $(\sigma_1-\sigma_2)$ is the difference between the principal stress. The stress-optic coefficient can be treated as a constant for each material. This law establishes that the difference in principal stress is proportional to the difference in the two refractive indices exhibited by the stressed material. For example, when light polarizations are incident on a birefringent material, the transmitted light has a phase shift between the polarizations because of the difference in the refractive indices (Fig. 1). The amount of this phase shift is called the retardation. If the stresses are constant throughout the thickness, the wave emerges with a retardation due to the refractive index difference given by equation (1):

$$R=C(\sigma_1-\sigma_2)d \quad (2)$$

where R is the retardation, and d is the specimen thickness[19].

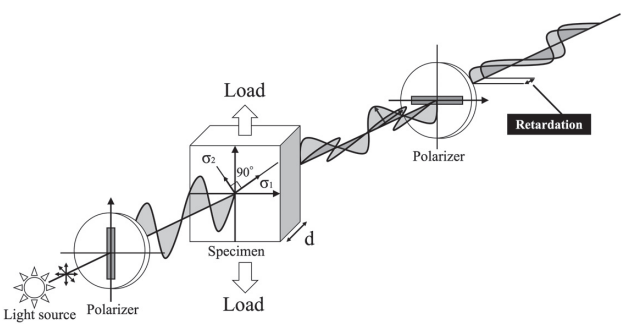

Fig. 1 Stress-optic law in photoelastic experiments.

Birefringence even occurs in transparent materials that are not inherently birefringent when stress or strain is applied, and the amount of retardation that occurs can be measured and then converted into a proportional stress. The near infrared 2D birefringence measurement system (WPA-200-NIR, Photonic Lattice, Miyagi, Japan) used in this study can investigate the internal strain and molecular orientation of a specimen, along with the stress distribution when stress is applied to the specimen. We can quantify such a stress by measuring the retardation of the transmitted light *via* the proportional relationship above. The optical setup of this system is illustrated in Fig. 2. The optical system consists of a light source, circular polarizer, wavelength filter, lens, imaging sensor, and camera. The near-infrared light emitted from the light source passes through the circular polarizer to become polarized light (Fig. 2A) and enters the loaded specimen (Fig. 2B). Because of the birefringence of the specimen, the incident light splits into two beams with different phase velocities in the specimen and passes through the specimen (Fig. 2C). Each light has a phase difference, and by passing this phase difference through a wavelength filter, only the isochromatic lines indicating the principal stress difference can be observed (Fig. 2D). These two isochromatic lines are combined by a polarizer and recorded by a camera (Fig. 2E). At this time, a color map is created according to the retardation obtained from the linearly polarized light component.

Verification of the proposed method using 2D birefringence measurement

The near infrared 2D birefringence measurement system is a device used to measure the retardation of light when an external force is applied to a transparent elastic material. Our study represents the first attempt to measure the properties of the aligner material using this equipment. Firstly, we verified whether it is possible to estimate the orthodontic force from the retardation measured when stress is generated in the aligner material. In the proposed method, the thermoplastic material was subjected to a pressurized molding force, which is the force used when the aligner was fabricated, and photoelasticity and mechanical properties were then measured. The force estimated by the birefringence measurement was compared with the

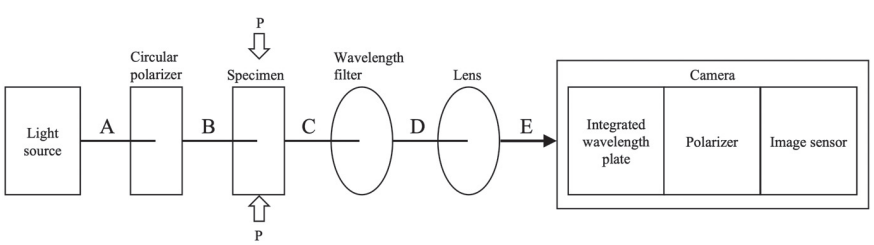

Fig. 2 Optical setup of the near infrared 2D birefringence measurement system.

actual mechanical properties. We adopted the commonly used tensile test for measuring the above-mentioned mechanical properties, which verifies the orthodontic force estimation by photoelasticity.

Specimen preparation

Specimens were prepared using a thermoplastic material, Erkodur (Erkodent Erich Kopp, Pfalzgrafenweiler, Germany), with a thickness of 0.8 mm. Erkodur is composed of glycol-modified PET. A trapezoidal pillar (20 mm high, 2 mm on the upper side, 16 mm on the lower side, and 40 mm deep) was made from hard plaster to simulate the four anterior maxillary teeth and the alveolar region of a dental model of an adult male (Fig. 3A, B), referring to a previous report[21]. This simplification is to make specimens with uniform thickness and to avoid the complex morphology of real dental models. The trapezoidal pillar was inserted into a pressure molding machine (Erkopress ci motion, Erkodent Erich Kopp) (Fig. 3C), and the thermoplastic material was then molded under pressure (Fig. 3D). The pressure-molding process was achieved by heating the material at 160°C for 45 s and cooling for 45 s under conditions recommended by the manufacturer. Next, the surface corresponding to the lingual side of the model was cut from the molded thermoplastic material with the cutter (Fig. 3E), and the cut material was then cut into strips 20.0 mm in length and 1.0 mm in width for use as measurement specimens (Fig. 3F). At this time, if the thermoplastic material was stretched on the model by application of a molding force that was not applied uniformly from the top to the bottom of the model, there was a concern that a slight difference in thickness would occur in different areas. Therefore, the specimens were cut out in a direction parallel to the direction of application of the molding force to prevent variations in the thickness.

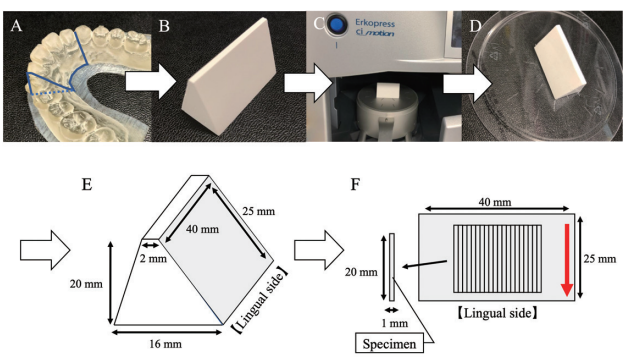

Fig. 3 Preparation of specimens.
(A) Dental model of an adult male; (B) trapezoidal column used to simulate the four anterior maxillary teeth; (C) trapezoidal column placed in a pressurized molding machine (Erkopress); (D) Erkodur 0.8 mm plate after pressurized molding; (E) cutout from the lingual side of a pressurized Erkodur 0.8 mm trapezoid; (F) specimen cut from the lingual side parallel to the direction of application of the molding force (red arrow).

Photoelasticity measurement

We measured the retardation with respect to the displacement for seven specimens (n=7) using the near infrared 2D birefringence measurement system (Fig. 4). We fabricated a fixing jig (Fig. 5) to apply specific displacement to the specimen. The specimen was fixed to the jig and pulled in the tensile direction at increasing intervals of 5 µm. The measured values were then acquired using birefringence analysis software (WPA-View Ver. 2.4.8.7, Photonic Lattice).

Measurement of mechanical properties

A tensile test was performed (n=7) using a dynamic

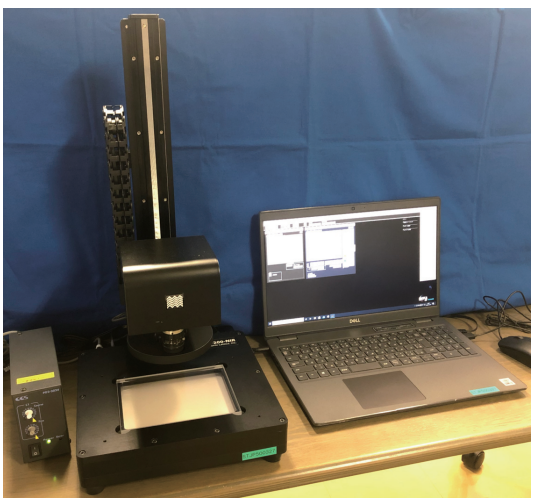

Fig. 4 Near infrared 2D birefringence measurement system (WPA-200-NIR).

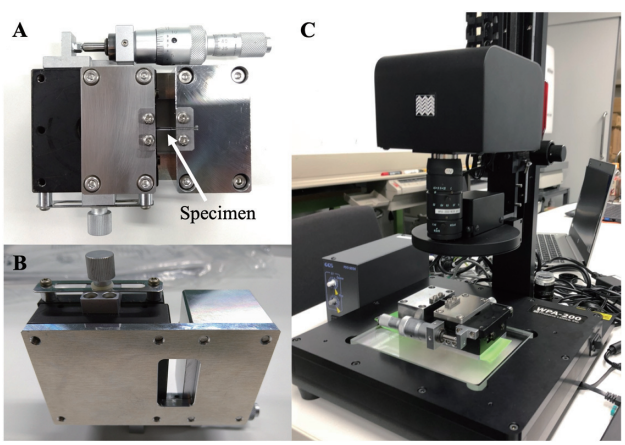

Fig. 5 Jig used for retardation measurements.
(A) Top view, showing the gap where the specimen is fixed; the displacement is defined using screws; (B) bottom view, where holes have been drilled to allow light to pass through; (C) the jig position is defined and the specimen is placed in the 2D birefringence measurement system.

mechanical analyzer (DMS6100, Hitachi High-Tech Science, Tokyo, Japan), and the load was measured with respect to the displacement. The applied load was gradually changed from 98 to 5,000 mN with a stress rate of 100 mN/min.

Optical retardation mapping

Given that the distribution of orthodontic force can be converted from the retardation map, we visualized the 2D retardation distribution when stress was applied to the specimen (*i.e.*, when a specified amount of displacement was applied). Birefringence analysis software was used to perform the mapping process.

Statistical analysis

When statistical tests were performed, the significance level was set at α=0.05 (for both sides), and p<0.05 was considered to be significant. SPSS Statistics 26 software (IBM, Armonk, NY, USA) was used to perform the statistical analysis.

RESULTS

Photoelastic properties by 2D birefringence measurement

Figure 6 shows the photoelastic properties measured with the near infrared 2D birefringence measurement system. The vertical axis represents the retardation and the horizontal axis represents the displacement. When the amount of displacement increased by 5 μm, the retardation increased almost constantly and showed a linear proportional relationship.

Mechanical properties of pressure-molded thermoplastic materials (tensile tests)

Figure 7 shows the measured mechanical properties of the thermoplastic materials after the pressurized molding. The vertical axis represents the load and the horizontal axis represents the displacement. The graph remains nonlinear for displacements up to 30 μm, but becomes linear at displacements above 30 μm. Therefore, we decided to extract the data recorded at displacements of more than 30 μm, which showed linearity. The graph produced after this data extraction process showed a linear elastic response, as illustrated in Fig. 8.

Relationship between applied load and retardation

Using the above results, we formulated two relationships with the common displacement: the relationship between the displacement and the retardation from the birefringence measurement, and the relationship between the displacement and the load of the tensile test. Based on these relationships, the conversion formula was introduced to translate the measured retardation into the applied load. The valid displacement range of the conversion formula was 0 to 100 μm, which is limited by the range of the birefringence measurement.

Pearson's correlation coefficient between the displacement and the retardation ranged from 0.997 to 1.000, and the two factors showed a strong positive correlation.

This regression equation is expressed as follows using the regression coefficient a_1 and the intercept c_1:

$$\text{Retardation (nm)} = a_1 \times \text{displacement (μm)} + c_1 \quad (1)$$

The regression coefficients of the displacement with respect to the retardation ranged from 6.234 to 7.322; both of these values were statistically significant,

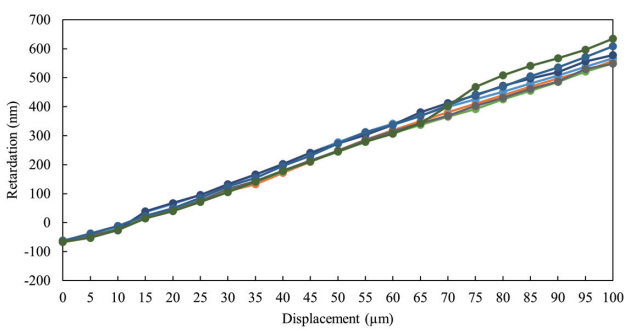

Fig. 6 Results of the photoelasticity measurement (n=7). The relationship between the retardation and the displacement remains linear over the entire displacement range.

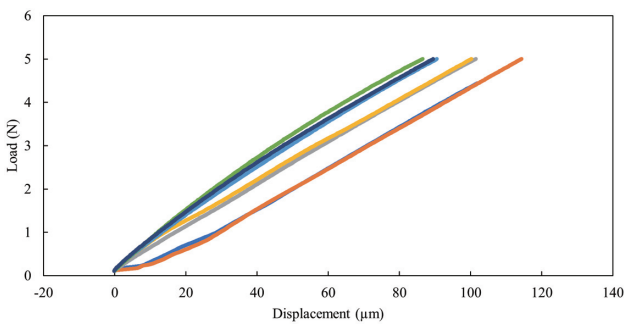

Fig. 7 Mechanical measurement results showing load versus displacement (n=7). The graph is nonlinear for displacements of up to 30 μm, but it becomes linear at displacements above 30 μm.

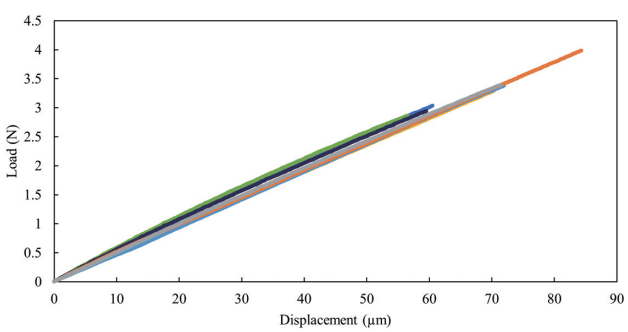

Fig. 8 Mechanical measurement results for displacements of more than 30 μm (n=7). The relationship between the retardation and the displacement remains linear over the entire displacement range.

resulting in a_1=6.610±0.375SD. The intercept of the regression equation was in the range from −61.4 to −104.0, and c_1=−76.4±13.5SD.

In the mechanical property measurement, Pearson's correlation coefficient of the displacement and the load showed a value ranging from 0.999 to 1.000, and the two parameters showed a strong positive correlation.

This regression equation is expressed as follows using the regression coefficient a_2 and the intercept c_2:

$$\text{Load (cN)} = a_2 \times \text{displacement (μm)} + c_2 \quad (2)$$

The regression coefficients of the displacement with respect to the load ranged from 4.626 to 5.062; both of these values were statistically significant, resulting in a_2=4.830±0.171SD. The intercept of the regression equation was within the range from −1.22 to 8.11, and c_2=4.20±2.92SD.

Therefore, the following relational equation between retardation and load can be obtained from equations (1) and (2):

$$\text{Retardation (nm)} = (a_1/a_2) \times \text{load (cN)} + (c_1 - (a_1/a_2) \times c_2) \quad (3)$$

The coefficient (a_1/a_2) expressed using the relational equation above over the seven specimen was 1.369±0.077SD, and the coefficient of variation (SD/average value) was 5.6%, which was quite a small value. In addition, there were no cases of rejection when the Smirnov-Grubbs rejection test was performed, and it was thus confirmed that the seven tests in this study showed stable results.

Finally, the constants in the relational equation were determined as follows:

$$\text{Retardation (nm)} = 1.401 \times \text{load (cN)} - 85.852 \quad (4)$$

Figure 9 shows the load–displacement curve from the mechanical and photoelasticity measurements using equation (4). The curve measured by photoelasticity tests *via* equation (4) was identical to the true curve obtained by the mechanical tests.

Sample size (power analysis)

From the results of this study, the sample size required to perform the equivalence test to confirm the hypothesis that the results from the photoelasticity and mechanical measurements do not differ was obtained as shown below.

The numerical results of the photoelasticity and mechanical measurements are presented in Table 1.

Equivalence in this case means that (1) the slope of the regression equation of the load and the displacement in the mechanical measurement, and (2) the slope of the regression equation of the load and the displacement for the conversion result obtained by converting the retardation into the load in the photoelasticity measurement, are equivalent.

Next, a practical definition is provided under the following conditions that demonstrates that the slopes of regression equations (1) and (2) presented above are equivalent.

Equivalent definition:

"The case where the ratio of (1) to (2) has a value of between 0.999 and 1.001 is equivalent."

The number of samples required to confirm the equivalence based on the definition above (*i.e.*, the number of combinations of the two measurements) was calculated as shown below.

When the significance level α=0.05 and the power=0.9 are adopted as the calculation conditions, a required sample size of four was obtained. In other

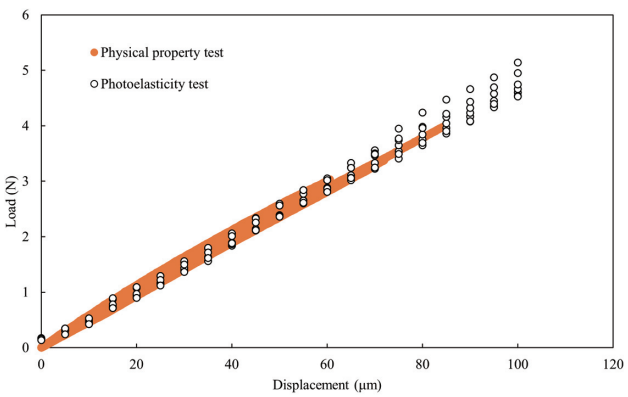

Fig. 9 Results of photoelasticity and mechanical measurements.
The retardation and load showed a strong relationship with respect to the displacement.

Table 1 Slopes of the regression equation for photoelasticity and mechanical properties measurement data

	Slope of regression equation	
Test number	(1) Physical properties test	(2) Photoelasticity test
1	4.739	4.741
2	4.686	4.688
3	4.758	4.756
4	4.626	4.627
5	5.027	5.026
6	5.062	5.062
7	4.912	4.913

words, in the case of a power of 0.9, if the accuracy of the test is ensured, then the sample size requirements can be satisfied by performing four sets of tests.

Therefore, the number of tests performed in this study (seven tests) was sufficient to confirm the equivalence.

Correlation coefficient of load and retardation

The overall relationship between the load and the retardation obtained for all the seven specimens was r=0.989, the significance probability was <0.001 in terms of Pearson's correlation coefficient, and a strong positive correlation was observed (Fig. 10).

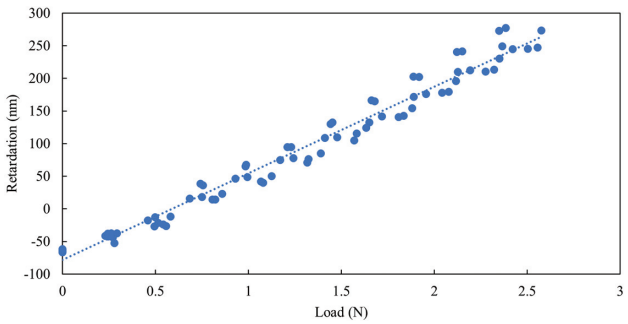

Fig. 10 Correlation between the photoelastic stress analysis (vertical axis: retardation) and the mechanical properties (horizontal axis: load).
The results show the correlation between the retardation and the load for each 5 μm increase in the displacement (maximum: 50 μm). Pearson's correlation coefficient r=0.989 and p<0.001, indicating a strong positive correlation.

Optical retardation mapping

Figure 11 shows the results of mapping of the two-dimensional retardation distribution when stress was applied to the specimen.

The magnitude of the retardation observed for each displacement is shown in a color graph, where the horizontal axis is displacement. Higher retardation is indicated by a darker red color, and lower retardation is indicated by a darker blue color. As can be seen, as the displacement increases, the color of the sample turns from blue to red, and the retardation increases can be visually confirmed.

DISCUSSION

If the orthodontic force exerted by an orthodontic appliance can be measured, then the relationship between tooth movement and the orthodontic force can be clarified in greater detail. However, to date, it has not been possible to accurately measure the orthodontic force with aligners because of the complex shape and the material of the appliance. Furthermore, a method to measure the actual orthodontic force in each individual living body has not yet been developed for use by other methods. In this study, we have proposed a method to measure the force of a transparent aligner-type orthodontic appliance and have confirmed the accuracy

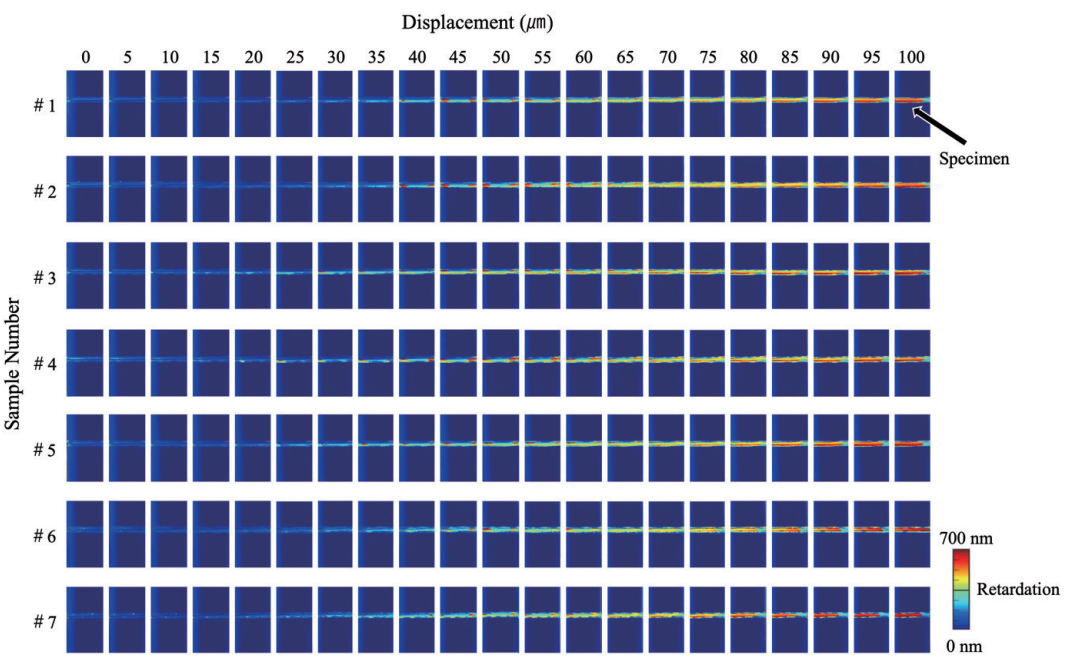

Fig. 11 Visualization of the optical retardation distribution.
The magnitude of the retardation for each displacement is shown in color maps. Higher retardation is indicated by a darker red shade, and lower retardation is indicated by a darker blue shade.

of this method.

Photoelastic stress analysis was used in this study for transparent specimens. In recent years, the application of photoelastic stress analysis has become increasingly widespread in studies of oral biomechanics[22-27]. In addition, the near infrared 2D birefringence measurement system employed in this study is believed to be useful for measuring the orthodontic force of aligners because it is simple, nondestructive, and offers the feature of real-time measurement. However, no previous studies have measured the orthodontic force of aligners *via* photoelasticity. Therefore, we measured the actual mechanical properties of the aligner materials to validate the effectiveness of our force estimation method using photoelasticity.

The results of this validation showed a strong relationship between the retardation and the load for the specified displacement. Furthermore, the equivalence test showed that the equivalence was valid, and a strong positive correlation (r=0.989) was observed in Pearson's correlation coefficient. Therefore, the retardation values measured using the near infrared 2D birefringence measurement system also reflected the mechanical properties of the aligner materials, and they were shown to be useful for measurement of the orthodontic forces generated by the aligner materials.

We confirmed that the retardation increased linearly in tandem with increasing displacement. This indicates that the displacement and the retardation are proportional to each other. Non-zero initial retardation without displacement (0 μm) in the displacement–retardation curve (Fig. 6) was due to the inherent material birefringence and the internal stress generated by molding.

In the tensile test, the curve shows nonlinearity up to a displacement of 30 μm, which is caused by an unintentional deflection when the specimen is mounted on the apparatus, and the tensile force is applied accurately after the deflection has been eliminated.

In both measurements, when the displacement increased, slight variations were observed in both the retardation value and the load amount for each specimen. These variations might be caused by the reproducibility of the pressure molding, such as local thickness differences of the material and subtle differences in temperature during heating.

The Erkodur plate (glycol-modified PET), which is formed as an aligner after pressurization, is stretched during processing, and it is thus assumed that its thickness slightly varies. Because the calculation from retardation to stress is affected by the specimen thickness, it will be necessary to consider the variations in thickness that occur in different parts of the aligner, and which part of the aligner should be measured in future work; we are currently conducting further research into this issue.

The amount of retardation for each amount of displacement was shown on a color map, providing a visual understanding of how the color distribution varied as the mechanical tensile stress was applied. Visualization of the orthodontic force of the aligner will enable instantaneous comparison of the magnitude and distribution of this force, and it is expected to enable prediction of the clinical response required to various tooth movements.

CONCLUSION

To provide appropriate aligner treatment to orthodontic patients, it is necessary to understand the characteristics of the orthodontic forces that are generated by aligners. In this study, we proposed the application of a 2D birefringence measurement method to measure the orthodontic forces generated by the aligner materials. This method enables simple and rapid measurement and provides a visual understanding of the orthodontic force without requiring any modification of the aligner or the model itself. Therefore, the proposed method will enable quantitative measurement of the influence on the orthodontic force of the material characteristics of the aligner, the edge shape, the material fatigue caused by attachment and removal of the device, and the temporal changes in the material.

ACKNOWLEDGMENTS

We would like to thank Mr. David MacDonald, MSc, from Edanz (https://jp.edanz.com/ac) for editing a draft of this manuscript and Mr. Kazutaka Takahashi of Seiko I Techno Research Inc. for his cooperation in performing the physical properties tests.

REFERENCES

1) The number of adults seeking orthodontic treatment in the UK continues to rise. Br Dent J 2018; 224: 847.
2) Pabari S, Moles DR, Cunningham SJ. Assessment of motivation and psychological characteristics of adult orthodontic patients. Am J Orthod Dentofacial Orthop 2011; 140: e263-272.
3) Jeremiah HG, Bister D, Newton JT. Social perceptions of adults wearing orthodontic appliances: A cross-sectional study. Eur J Orthod 2011; 33: 476-482.
4) Boyd RL, Miller RJ, Vlaskalic V. Three-dimensional diagnosis and orthodontic treatment of complex malocclusions with the Invisalign appliance. Semin Orthod 2001; 7: 274-293.
5) Kuo E, Miller RJ. Automated custom-manufacturing technology in orthodontics. Am J Orthod Dentofacial Orthop 2003; 123: 578-581.
6) Miller KB, McGorray SP, Womack R, Quintero JC, Perelmuter M, Gibson J, *et al*. A comparison of treatment impacts between Invisalign aligner and fixed appliance therapy during the first week of treatment. Am J Orthod Dentofacial Orthop 2007; 131: 302.e1-9.
7) Rossini G, Parrini S, Castroflorio T, Deregibus A, Debernardi CL. Periodontal health during clear aligners treatment: A systematic review. Eur J Orthod 2015; 37: 539-543.
8) Fang X, Qi R, Liu C. Root resorption in orthodontic treatment with clear aligners: A systematic review and meta-analysis. Orthod Craniofac Res 2019; 22: 259-269.
9) Barbagallo LJ, Jones AS, Petocz P, Darendeliler MA. Physical properties of root cementum: Part 10. Comparison of the effects of invisible removable thermoplastic appliances with light and heavy orthodontic forces on premolar cementum. A

microcomputed-tomography study. Am J Orthod Dentofacial Orthop 2008; 133: 218-227.
10) Kravitz ND, Kusnoto B, BeGole E, Obrez A, Agran B. How well does Invisalign work? A prospective clinical study evaluating the efficacy of tooth movement. Am J Orthod Dentofacial Orthop 2009; 135: 27-35.
11) Djeu G, Shelton C, Maganzini A. Outcome assessment of Invisalign and traditional orthodontic treatment compared with the American Board of Orthodontics objective grading system. Am J Orthod Dentofacial Orthop 2005; 128: 292-298; discussion 298.
12) Bollen AM, Huang G, King G, Hujoel P, Ma T. Activation time and material stiffness of sequential removable orthodontic appliances. Part 1: Ability to complete treatment. Am J Orthod Dentofacial Orthop 2003; 124: 496-501.
13) Lombardo L, Arreghini A, Ramina F, Huanca Ghislanzoni LT, Siciliani G. Predictability of orthodontic movement with orthodontic aligners: A retrospective study. Prog Orthod 2017; 18: 35.
14) Iijima M, Kohda N, Kawaguchi K, Muguruma T, Ohta M, Naganishi A, *et al*. Effects of temperature changes and stress loading on the mechanical and shape memory properties of thermoplastic materials with different glass transition behaviours and crystal structures. Eur J Orthod 2015; 37: 665-670.
15) Skaik A, Wei XL, Abusamak I, Iddi I. Effects of time and clear aligner removal frequency on the force delivered by different polyethylene terephthalate glycol-modified materials determined with thin-film pressure sensors. Am J Orthod Dentofacial Orthop 2019; 155: 98-107.
16) Elkholy F, Schmidt F, Jäger R, Lapatki BG. Forces and moments delivered by novel, thinner PET-G aligners during labiopalatal bodily movement of a maxillary central incisor: An in vitro study. Angle Orthod 2016; 86: 883-890.
17) Son HJ, Lee KH, Sim JY, Kim HY, Kim JH, Kim WC. Pressure differences from clear aligner movements assessed by pressure sensors. Biomed Res Int 2020; 2020: 8376395.
18) Eugene H. Optics. 5th ed. New York: Pearson Education; 2016. pp. 380-381.
19) Kuske A. Photoelastic stress analysis. London, New York: John Wiley & Sons; 1974. pp. 86-104.
20) Rajpal SS. Introduction to optical metrology. Boca Raton: CRC Press; 2016. pp. 182-192.
21) Ryu JH, Kwon JS, Jiang HB, Cha JY, Kim KM. Effects of thermoforming on the physical and mechanical properties of thermoplastic materials for transparent orthodontic aligners. Korean J Orthod 2018; 48 :316-325.
22) Zanatta LC, Dib LL, Gehrke SA. Photoelastic stress analysis surrounding different implant designs under simulated static loading. J Craniofac Surg 2014; 25: 1068-1071.
23) da Silva DP, Cazal C, de Almeida FC, Dias RB, Ballester RY. Photoelastic stress analysis surrounding implant-supported prosthesis and alveolar ridge on mandibular overdentures. Int J Dent 2010; 2010: 780670.
24) de Castro Ferreira E, Corbella S, Zanatta LC, Taschieri S, del Fabbro M, Gehrke SA. Photo-elastic investigation of influence of dental implant shape and prosthetic materials to patterns of stress distribution. Minerva Stomatol 2012; 61: 263-272.
25) Assunção WG, Barão R, Adelino V, Tabata LF, Gomes ÉA, Delben JA, *et al*. Biomechanics studies in dentistry: Bioengineering applied in oral implantology. J Craniofac Surg 2009; 20: 1173-1177.
26) Yamamoto M, Miura H, Okada D, Komada W, Masuoka D. Photoelastic stress analysis of different post and core restoration methods. Dent Mater J 2009; 28: 204-211.
27) Baena Lopes M, Romero Felizardo K, Danil Guiraldo R, Fancio Sella K, Ramos Junior S, Gonini Junior A, *et al*. Photoelastic stress analysis of different types of anterior teeth splints. Dent Traumatol 2021; 37: 256-263.